Numerical prediction of dispersed turbulent liquid–solid flows in vertical pipes

GIANANDREA V. MESSA, Post-Doctoral Research Assistant, *DICA, Politecnico di Milano, Milano, Italy*
Email: gianandreavittorio.messa@polimi.it (author for correspondence)

STEFANO MALAVASI, Assistant Professor, *DICA, Politecnico di Milano, Milano, Italy*
Email: stefano.malavasi@polimi.it

1 Introduction

Many engineering applications involve the presence of solid particles with moderate loading ratios in a turbulent liquid pipe flow, for example the oil plants. These flows are characterized by the fact that the particles move as individual entities under the effects of gravity and of the interactions among particles, fluid and solid walls. According to Loth (2011), these flows are referred to as "dispersed" and occur when the solid volume fraction is lower than 0.10. The effect of small-scale turbulent eddies has a strong influence on the particle motion; therefore, the interaction between the turbulence characteristics of the fluid and the particles is very significant. Fluid–particle interactions are particularly important in dispersed liquid–solid flows which, compared with gas–solid flows, are characterized by lower particle Stokes number S_θ and higher microscale Reynolds number R_θ. S_θ and R_θ are defined as

$$\mathsf{S}_\theta = \frac{\rho_p d_p \sqrt{\overline{\boldsymbol{u}'_p \boldsymbol{u}'_p}}}{9\rho_f \nu}, \quad \mathsf{R}_\theta = \frac{d_p \sqrt{\overline{\boldsymbol{u}'_p \boldsymbol{u}'_p}}}{\nu} \tag{1}$$

where ρ_p and ρ_f are the densities of the particles and the fluid, d_p is the particle size, ν is the kinematic viscosity coefficient of the fluid, and $\boldsymbol{u}'_p$ is the fluctuating velocity vector of the particles, which will be reintroduced later.

Turbulent dispersed liquid–solid flows in pipes have been rarely addressed either experimentally (Zisselmar and Molerus 1979, Nouri *et al.* 1987, Alajbegovic *et al.* 1994, Assad *et al.* 2000, Hosokawa and Tomiyama 2004, Sad Chemloul and Benrabah 2008, Pepple 2010) or computationally (Alajbegovic *et al.* 1999, Hadinoto 2010, Hadinoto and Chew 2010). Focusing on numerical investigations, both Eulerian–Lagrangian and Eulerian–Eulerian models have been used. In both groups, the fluid phase is considered to be a continuous mean. In Eulerian–Lagrangian models, the solid phase is simulated by following the trajectories of all the particles; in Eulerian–Eulerian models (referred to as "two-fluid" models), the solid phase is treated as a second continuous interpenetrating fluid. The modelling of some physical mechanisms, such as particle–particle and particle–wall interactions, is more straightforward with the Eulerian–Lagrangian approach, but a large number of particles trajectories are required to achieve statistically stationary values of the average flow variables, which are instead directly produced as output of the two-fluid models. This results in a higher computational cost compared with two-fluid models. Moreover, Frawley *et al.* (2010) compared the two approaches for a nearly

Received 29 July 2013; accepted 16 June 2014/Open for discussion until 30 April 2015.

dense liquid–solid flows in a sudden enlargement and found that the two-fluid model allows a better prediction of the fluid turbulent kinetic energy downstream the singularity where the flow returns to equilibrium. The two-fluid approach was therefore judged the most appropriate for the flows examined here.

The proper modelling of the interactions among fluid, particles and walls is essential for achieving reliable predictions. Following a well-established approach described by Burns *et al.* (2004), most of the two-fluid models reported in the literature (Spalding 1980, Issa and Oliveira 1997, Frawley *et al.* 2010, Hadinoto 2010, Hadinoto and Chew 2010) account for turbulence by averaging and Reynolds-decomposing the local instant conservation equations. The flow variables are expressed as the sum of an average value and a fluctuation and additional terms arise, for example, from the correlations between fluctuating velocities and fluctuating volume fractions. Two interfacial momentum transfer terms $\boldsymbol{M}_f$ and $\boldsymbol{M}_p$ are introduced in the momentum equations for the fluid and particle phases, indicated by the subscripts f and p in this paper. If the force of the fluid on the particle is restricted to the form drag and the particles are spherical, these terms are given by

$$\boldsymbol{M}_f = -\boldsymbol{M}_p = \frac{(\rho_p + C_{vm}\rho_f)\alpha_p}{\tau_p}(\boldsymbol{U}_p - \boldsymbol{U}_f) \tag{2}$$

where C_{vm} is the virtual mass coefficient, commonly taken as 0.5, α_p is the average local volume fraction of the particles, $\boldsymbol{U}_p$ and $\boldsymbol{U}_f$ are the average velocity vectors of the particles and the fluid, and τ_p is the response time of a particle, which is a typical timescale of the particle's reaction to changes in the average fluid velocity. τ_p may be evaluated as

$$\tau_p = \frac{4}{3}\frac{(\rho_p + C_{vm}\rho_f)d_p}{\rho_f C_d U_r} \tag{3}$$

where U_r is the modulus of the difference between the average velocities of the phases and C_d is the drag coefficient, commonly expressed as a function of the particle Reynolds number $\mathrm{R_p} = d_p U_r/\nu$.

Turbulent dispersion and turbulence modulation arise from the interactions between the particles and the turbulent fluid. Turbulent dispersion is commonly associated with the correlations between the fluctuating velocity vector and the fluctuating volume fraction of each phase; these terms are referred to as $\boldsymbol{u}'_q$ and α'_q, where the subscript q is a phase indicator parameter which is equal to f for the fluid and to p for the particles. The terms $\overline{\alpha'_q \boldsymbol{u}'_q}$ are typically modelled by the eddy diffusivity hypothesis:

$$\overline{\alpha'_q \boldsymbol{u}'_q} = \frac{\nu_{t,f}}{\sigma_\alpha}\nabla\alpha_q \tag{4}$$

where $\nu_{t,f}$ is the eddy viscosity of the fluid and σ_α is the turbulent Schmidt number for volume fractions, usually treated as a calibration parameter.

The presence of particles can affect the turbulence of the fluid. This extremely complex phenomenon, referred to as turbulence modulation, does not seem to be completely understood at present but, basically, the experimental evidence indicates that small particles tend to attenuate turbulence whilst large particles augment it (Crowe 2000, Hosokawa and Tomiyama 2004). In most two-fluid models, turbulence modulation is accounted for by adding source terms in the conservation equations for the turbulent kinetic energy of the fluid k and its dissipation rate ε, referred to as S_{kp} and $S_{\varepsilon p}$, respectively. Mandø *et al.* (2009) classify the physically-based models for these terms according to approach followed, namely:

- *Standard approach*. The source term in the k equation due to the presence of particles is calculated by multiplying the momentum equation by $\boldsymbol{U}_f$ and applying a Reynolds averaging procedure. After subtracting the mean kinetic energy, the following expression for S_{kp} is obtained:

$$S_{kp} = \frac{\alpha_p\rho_p}{\tau_p}(\overline{\boldsymbol{u}'_f\boldsymbol{u}'_p} - 2k) \tag{5}$$

  The additional dissipation due to the particles $S_{\varepsilon p}$ is instead assumed proportional to the similar term in the k equation:

$$S_{\varepsilon p} = C_{3\varepsilon}\frac{\varepsilon}{k}S_{kp} \tag{6}$$

  in which $C_{3\varepsilon}$ is a numerical constant. Lightstone and Hodgson (2004) listed several models of this category which distinguish from the way in which the correlation $\overline{\boldsymbol{u}'_f\boldsymbol{u}'_p}$ is evaluated as well as the value attributed to $C_{3\varepsilon}$ (actually almost always very close to one).
- Consistent approach, in which the product of the average velocity and the momentum equation are subtracted from the mechanical energy conservation equation, resulting in the following expression for S_{kp}:

$$S_{kp} = \frac{\alpha_p\rho_p}{\tau_p}[U_r^2 + \overline{\boldsymbol{u}'_p\boldsymbol{u}'_p} - \overline{\boldsymbol{u}'_f\boldsymbol{u}'_p}] \tag{7}$$

  whilst $S_{\varepsilon p}$ is obtained from Eq. (6) with $C_{3\varepsilon} = 1.8$ (Lain and Sommerfeld 2003).
- Mixed approach of Mandø *et al.* (2009) in which, through a theoretical derivation, S_{kp} is achieved by adding the source terms of the two other approaches (Eqs. 5 and 7):

$$S_{kp} = \frac{\alpha_p\rho_p}{\tau_p}[U_r^2 + \overline{\boldsymbol{u}'_p\boldsymbol{u}'_p} - 2k] \tag{8}$$

  whist $S_{\varepsilon p}$ is obtained from Eq. (6) with $C_{3\varepsilon} = 1.0$. The mixed approach may result in either positive or negative values of S_{kp} according to the relative weight of the three terms in Eq. (8). Mandø *et al.* (2009) neglected the correlation $\overline{\boldsymbol{u}'_p\boldsymbol{u}'_p}$ which was found to be small in their validation examples, but underlined

that this term may become important for dense flows and for wall-bounded flows.

A two-fluid model capable of predicting the behaviour of dispersed liquid–solid flows in pipes is still lacking at present. The studies of Hadinoto (2010) and Hadinoto and Chew (2010) seem to be the only examples in which a two-fluid model is applied to these flows and the numerical predictions are compared with experimental data. The authors underlined the key role played by the drag coefficient correlation and the source terms S_{kp} and $S_{\varepsilon p}$, but failed in identifying a unique combination of these parameters which produces good agreement with the experimental evidence for different flow conditions. This unfortunately limits the use of their model as a predictive tool for engineering purposes unless a calibration is made on a case-by-case basis.

In this paper we present a new two-fluid model, developed starting from the works of Hadinoto (2010) and Hadinoto and Chew (2010). By comparison with the experimental data of Alajbegovic *et al.* (1994) and Hosokawa and Tomiyama (2004), the proposed model proved that it is capable of reproducing the main features of the turbulent liquid–solid flow in vertical pipes for different flow conditions. The added value of this model relies on two main features. First, each sub-model is associated with a precise physical feature of the flow; by doing so, the same combination of sub-models procures good agreement with the experimental evidence without any calibration made on a case-by-case basis. Second, an extension of the source terms in the k and ε equations developed by Mandø *et al.* (2009) is proposed, which shows promising results for turbulence modulation in the case of liquid–solid flows. In particular, the model appears to be able to reproduce the effect of particle size on turbulence modulation, in agreement with the experimental results (Crowe 2000).

2 Mathematical model

2.1 *Two-fluid model*

The two-fluid model has been implemented in the commercial CFD code PHOENICS version 2011 by applying original modifications to the model developed by Spalding (1980) and embedded in the software.

The flow is assumed statistically steady and so the mass and momentum conservation equations for each phase are, respectively,

$$\nabla(\alpha_q \rho_q \boldsymbol{U}_q) - \nabla\left(\rho_q \frac{\nu_{t,f}}{\sigma_\alpha}\nabla\alpha_q\right) = 0 \tag{9}$$

$$\begin{aligned}\nabla(\alpha_q\rho_q\boldsymbol{U}_q\boldsymbol{U}_q) - \overbrace{\nabla(\alpha_q\rho_q\nu\nabla\boldsymbol{U}_q)}^{\text{only if } q=f} - \nabla(\alpha_q\rho_q\nu_{t,q}\nabla\boldsymbol{U}_q) \\ -\nabla\left(\boldsymbol{U}_q\rho_q\frac{\nu_{t,f}}{\sigma_\alpha}\nabla\alpha_q\right) = -\alpha_q\nabla P + \alpha_q\rho_q\mathbf{g} + \boldsymbol{M}_q\end{aligned} \tag{10}$$

where once again, the subscript q is a phase indicator parameter equal to f and p for the fluid and the particles, respectively. Moreover, P is the average pressure, $\nu_{t,q}$ is the eddy viscosity of phase q, and $\boldsymbol{g}$ is the gravitational acceleration vector. The turbulent Schmidt number for volume fraction σ_α is set to 1.5 as this is the value which procures the best agreement with the experiments. The interfacial momentum transfer term $\boldsymbol{M}_{q=f,p}$ includes drag, lift, and virtual mass forces:

$$\begin{aligned}\boldsymbol{M}_f = -\boldsymbol{M}_p = &\frac{(\rho_p + C_{vm}\rho_f)\alpha_p}{\tau_p}(\boldsymbol{U}_p - \boldsymbol{U}_f) \\ &+ \frac{6}{\pi}C_l\rho_f\alpha_p(\boldsymbol{U}_p - \boldsymbol{U}_f)(\nabla\boldsymbol{U}_f) \\ &+ C_{vm}\rho_f\alpha_p(\boldsymbol{U}_p\cdot\nabla\boldsymbol{U}_p - \boldsymbol{U}_f\cdot\nabla\boldsymbol{U}_f)\end{aligned} \tag{11}$$

and the lift coefficient, C_l, is set to 0.5. The particle response time, τ_p, is calculated by means of Eq. (3), in which C_d is evaluated by the formula of Dellavalle (1948) for a single particle in an infinite medium. Two correction factors proposed by Di Felice (1994) and Pinelli *et al.* (2004) account for the presence of multiple particles and the free stream turbulence of the carrier phase. The drag coefficient is finally given by

$$\begin{aligned}C_d = &\alpha_f^{2-\beta}\left(0.63 + 4.8\sqrt{\frac{1}{\mathrm{R_p}}}\right)^2 \\ &\times\left\{0.4\left[\tanh\left(16\frac{\lambda}{d_p} - 1\right)\right] + 0.6\right\}^{-2}\end{aligned} \tag{12}$$

where $\lambda = \sqrt[4]{\nu^3/\varepsilon}$ is the Kolmogorov length scale and β is a parameter depending upon $\mathrm{R_p}$ according to the following law:

$$\beta = 3.7 - 0.65\exp\left[-\frac{1}{2}(1.5 - \log(\mathrm{R_p}))^2\right] \tag{13}$$

The evaluation of C_d is a peculiar feature of our model.

The eddy viscosity of the fluid $\nu_{t,f}$ is evaluated by means of a modified formulation of the k–ε standard turbulence model:

$$\begin{aligned}\nabla(\alpha_f\rho_f\boldsymbol{U}_f k) = &\nabla\left[\alpha_f\rho_f\left(\nu + \frac{\nu_{t,f}}{\sigma_k}\right)\nabla k\right] \\ &+ \alpha_f\rho_f(2\nu_{t,f}\mathbf{D}_\mathrm{f} : \nabla\boldsymbol{U}_f - \varepsilon) \\ &+ \nabla\left[\rho_f\frac{\nu_{t,f}}{\sigma_\alpha}k\nabla\alpha_f\right] + \alpha_f S_{kp}\end{aligned} \tag{14}$$

$$\begin{aligned}\nabla(\alpha_f\rho_f\boldsymbol{U}_f\varepsilon) = &\nabla\left[\alpha_f\rho_f\left(\nu + \frac{\nu_{t,f}}{\sigma_\varepsilon}\right)\nabla\varepsilon\right] \\ &+ \alpha_f\rho_f\frac{\varepsilon}{k}(C_{1\varepsilon}2\nu_{t,f}\mathbf{D}_\mathrm{f} : \nabla\boldsymbol{U}_f - C_{2\varepsilon}\varepsilon) \\ &+ \nabla\left[\rho_f\frac{\nu_{t,f}}{\sigma_\alpha}\varepsilon\nabla\alpha_f\right] + \alpha_f S_{\varepsilon p}\end{aligned} \tag{15}$$

$$\nu_{t,f} = C_\mu\frac{k^2}{\varepsilon} \tag{16}$$

where $\mathbf{D}_f = 0.5[\nabla \boldsymbol{U}_f + (\nabla \boldsymbol{U}_f)^T]$ is the deformation tensor, and the model constants are the standard values, namely $\sigma_k = 1.0$, $\sigma_\varepsilon = 1.314$, $C_\mu = 0.09$, $C_{1\varepsilon} = 1.44$, and $C_{2\varepsilon} = 1.92$. The modelling of the source terms S_{kp} and $S_{\varepsilon p}$ accounting for turbulence modulation is another peculiar feature of our model. These terms are evaluated using an extended version of the model of Mandø *et al.* (2009) (Eqs. 6 and 8) which includes the correlation $\boldsymbol{u}'_p \cdot \boldsymbol{u}'_p$. This term is not solved via a transport equation, but evaluated from k by means of the algebraic model of Issa and Oliveira (1997):

$$\begin{aligned}
&\overline{\boldsymbol{u}'_p \boldsymbol{u}'_p} = 2k \frac{1 + \mathrm{S_T}(\Gamma - \gamma m_T/3)}{(1 + \mathrm{S_T}\Gamma)^2}, \quad \mathrm{S_T} = \frac{\tau_p}{T}, \\
&\Gamma = \sqrt{1 + (m_T \gamma)^2}, \quad \gamma = \frac{U_r}{\sqrt{2/3k}} \\
&\frac{T}{T_E} \cong 1 - \frac{1 - \beta_T}{1 + (\tau_p/T_E)^{0.4(1+0.01\tau_p/T_E)}}, \quad m_T = m\left(\frac{T}{T_E}\right), \\
&\beta_T = \frac{T_L}{T_E}, \quad m = \frac{T_E}{t_e}, \quad t_e = \frac{l_m}{\sqrt{2/3k}}
\end{aligned} \tag{17}$$

Besides the particle response time, τ_p, which has already been defined in Eq. (3), different time scales appear in Eq. (17), namely: the fluid integral time scale seen by a particle in the absence of relative velocity T; the Eulerian fluid time scale in a frame moving with the average fluid velocity T_E; the Lagrangian integral time scale of the fluid T_L; and the eddy turnover time t_e, defined with respect to the mixing length $l_m = C_\mu^{3/4} k^{3/2}/\varepsilon$. Five dimensionless variables ($\mathrm{S_T}$, m, m_T, β_T, and Γ) relate these time scales to each other and to a dimensionless crossing trajectories parameter γ. The values of β_T and m are not well defined in the literature. Here, we assumed the usual value $m = 1.0$, whilst β_T was set to 0.5 after verifying its minor influence on our numerical results.

The model of Issa and Oliveira (1997) prescribes the particle eddy viscosity $\nu_{t,p}$ to be equal to that of the fluid $\nu_{t,f}$ and the correlation $\overline{\boldsymbol{u}'_f \boldsymbol{u}'_p}$ to be equal to $\overline{\boldsymbol{u}'_p \boldsymbol{u}'_p}$. Therefore, we set $\nu_{t,p} = \nu_{t,f}$ in Eq. (10).

2.2 *Computational domain and boundary conditions*

The upward flow through different vertical pipes was simulated, exploiting the flow and geometrical symmetries of the phenomenon by solving only over a thin slice of the pipe with one cell in the azimuthal direction (Fig. 1).

A fully-developed turbulent flow profile was specified at the pipe inlet, with the distribution of the axial average velocity, turbulent kinetic energy and dissipation rate determined from Nikuradse's boundary-layer theory (Schlichting 1960) for the fully-developed single-phase flow in a pipe (Table 1). At the inlet section, the superficial velocities of the two phases V_f and V_p (which appear in the fully-developed profiles in Table 1) were set as reported in the experiments. The same applied to

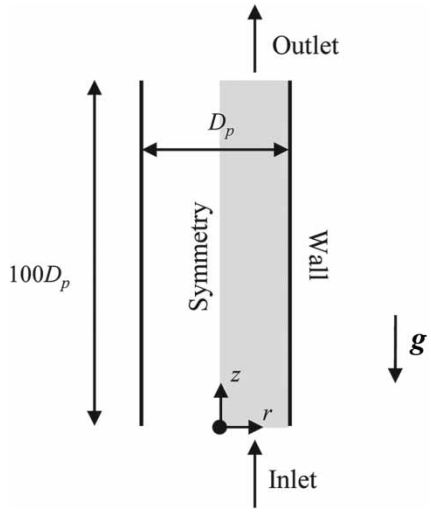

Figure 1 Computational domain and boundary conditions

Table 1 Fully-developed flow profile at inlet (from Nikuradse's boundary layer theory for fully-developed single-phase flow in a pipe)

Axial average velocity of phase $j = f, p$:

$$U_{z,j} = V_j \frac{(N_j + 1)(2N_j + 1)}{2N_j^2}\left(1 - \frac{2r}{D_p}\right)^{1/N_j} \qquad N_j = \frac{1}{\sqrt{f_j}}$$

$$f_j = [1.82 \log(\mathrm{R_j}) - 1.64]^{-2} \qquad \mathrm{R_j} = \frac{V_j D_p}{\nu}$$

Turbulent kinetic energy:

$$k = V_f^2 \frac{f_f}{8}\left[1 + \frac{2}{3}\frac{2r}{D_p} + \frac{10}{3}\left(\frac{2r}{D_p}\right)^3\right]$$

Dissipation rate:

$$\varepsilon = 0.1643 \frac{k^{3/2}}{l_{m,i}}$$

$$l_{m,i} = \frac{D_p}{2}\left[0.14 - 0.08\frac{2r}{D_p} - 0.06\left(\frac{2r}{D_p}\right)^4\right]$$

the area-averaged inlet solid volume fraction; the inlet solid volume fraction was assumed uniformly distributed. At the outlet, the normal gradients of all variables and the value of the pressure were set to zero.

The length of the computational domain was $100D_p$, where D_p is the pipe diameter, to ensure the attainment of fully-developed flow conditions, which was found to occur around $60D_p - 70D_p$ downstream of the inlet for all the flow conditions considered. The section at a distance of $90D_p$ downstream of the inlet was selected for comparison with the experiments. At the pipe wall, no slip conditions were imposed on the fluid phase, and the equilibrium log law of Launder and Spalding (1972) for smooth walls was employed for the velocities of the two phases, the turbulent kinetic energy of the fluid, and its dissipation rate in the near-wall cells. Attention was paid in guaranteeing the fulfilment of the condition $30 < y^+ < 130$, where y^+ is the non-dimensional distance of the first grid point from the walls; the value of y^+ was around 30 for all the flow conditions considered in this work.

Table 2 Flow conditions considered for comparison (A = Alajbegovic *et al.* 1994; H = Hosokawa and Tomiyama 2004)

Case	Particle	J_f (ms^{-1})	J_p (ms^{-1})	C (%)	S_θ (-)	R_θ (-)
A1	Ceramic/water: $\rho_p = 2450\,\mathrm{kg/m^3}$,	1.888	0.045	2.33	40	134
A2	$d_p = 2.32\,\mathrm{mm}$, and $D_p = 30.6\,\mathrm{mm}$	2.196	0.060	2.66	36	130
H1	Ceramic/water: $\rho_p = 3200\,\mathrm{kg/m^3}$,	0.500	0.002	0.70	32	90
H2	$d_p = 1.0\,\mathrm{mm}$ (H1–H2),	0.500	0.004	1.00	37	103
H3	$d_p = 2.5\,\mathrm{mm}$ (H3), and $D_p = 30\,\mathrm{mm}$	0.500	0.002	0.80	75	210

2.3 *Computational methodology and consistency of the numerical solution*

The calculations were performed following the elliptic-staggered formulation in which the scalar variables are evaluated at the cell centres and the velocity components at the cell faces. Central differencing was employed for the diffusion terms, whilst the convection terms were discretized using the hybrid scheme of Spalding (1972). The finite-volume equations were solved iteratively by means of the IPSA algorithm of Spalding (1980). Inertial relaxation was applied to the momentum equations with a false time step of 0.01 s, and a linear relaxation factor of 0.4 was applied to all other flow variables.

A cylindrical-polar structured mesh was used to discretize the domain. Grid independence studies were performed on a specific flow condition – referred to as A1 in Table 2 – by using three different meshes, as follows: 20 by 150 cells along the radial and the axial directions, respectively (Grid 1); 30 by 200 (Grid 2); and 40 by 300 (Grid 3). In compliance with the consistency of the boundary conditions, meshes with uniformly distributed cells have been considered. The grid discretization error on the fine grid solution at a distance of $90D_p$ from the inlet section was evaluated following the guidelines of Celik *et al.* (2008), and was found to be generally lower than about 0.75% for the average and root mean square (RMS) velocities of both phases and 1.7×10^{-4} (abs) for the solid volume fraction. Actually, in the near-wall region, the uncertainty on the fluid RMS velocity – which is the parameter most susceptible to the grid discretization level – reaches a local peak of about 1.6%, which corresponds to only 0.002 m/s. Grid 3 was thus judged capable in providing a numerically consistent solution.

3 Results and discussion

The numerical predictions were compared with experimental data reported by Alajbegovic *et al.* (1994) and Hosokawa and Tomiyama (2004). Details of the flow conditions simulated are summarized in Table 2, in which

$$J_f = V_f(1 - C), \quad J_p = V_p C \tag{18}$$

are the volumetric fluxes of fluid and solids, respectively, and C is the area-averaged solid volume fraction. The same table reports also the Stokes number S_θ and microscale Reynolds number R_θ (Eq. 1) at the pipe centre. The moderate values of S_θ and relatively large values of R_θ underline the important role of fluid–particle interactions, and therefore the significance of these cases for validating the proposed model.

The capability of this model to reproduce the main features of the flow is first checked by reference to a couple of scenarios investigated experimentally by Alajbegovic *et al.* (1994) regarding the upward flow of water and ceramic particles. Details of the flow conditions considered for comparison, referred to as A1 and A2, are given in Table 2.

Figure 2a–d compares the predicted and measured radial profiles of axial average velocity and RMS velocity of both phases. Unfortunately, Alajbegovic *et al.* (1994) did not report measurements of the azimuthal velocity fluctuations which we supposed to be equal to the radial velocity fluctuations, like Hadinoto and Chen (2010) did. The plots indicate that the model is capable in procuring accurate estimation of the axial components of the average velocity of the fluid and the particles (referred to as U_{fz} and U_{pz}, respectively), the deviations from the experimental data being below 5% (Fig. 2a,b). Also the RMS velocity of the fluid ($u_{\mathrm{RMS},f}$) seems roughly well predicted; the model slightly underestimates the measurements, with a maximum deviation of about 15% (Fig. 2c). The predicted values of particle RMS velocity ($u_{\mathrm{RMS},p}$) are in rather good agreement with the experimental evidence in the turbulent core region of the pipe, whilst an underestimation occurs close to the pipe wall (Fig. 2d). Further research is needed to improve the quality of the predictions close to the pipe wall, especially for high values of solid volume fraction. This is the most critical feature of the proposed model.

The model's validation is extended to the radial profile of solid volume fraction in Fig. 2e, where the $\pm 10\%$ error bars here correspond to the uncertainty reported by the experimenters. The good agreement between computations and measurements further confirms the reliability of the model.

Reference is now made to one of the peculiar features of turbulent dispersed liquid–solid flows, which is turbulence modulation. It is a commonly followed practice (Hosokawa and Tomiyama 2004, Sad Chemloul and Benrabah 2008, Hadinoto

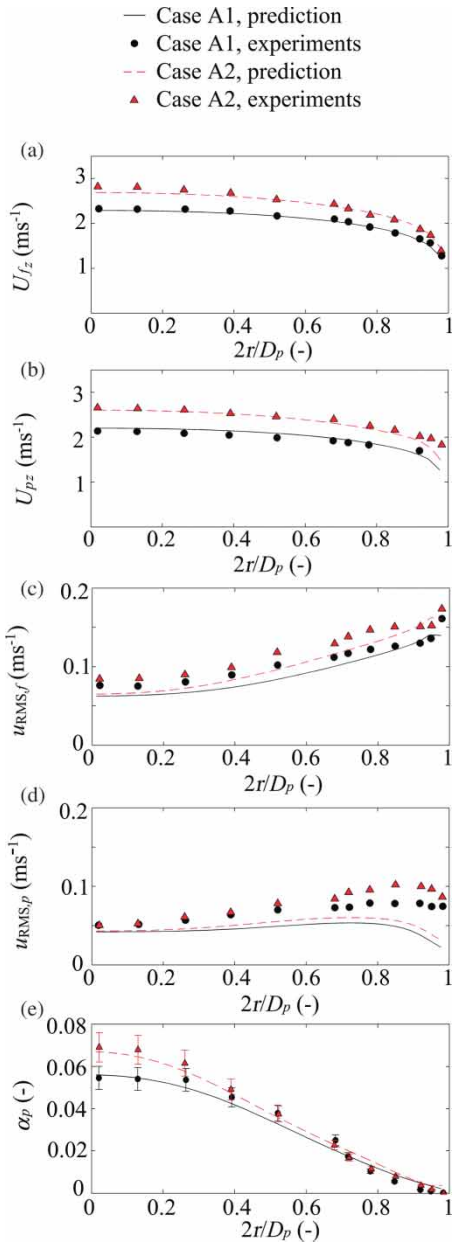

Figure 2 Comparison between numerical predictions and experimental data (Alajbegovic *et al.* 1994) for the flow conditions A1 and A2 in Table 2

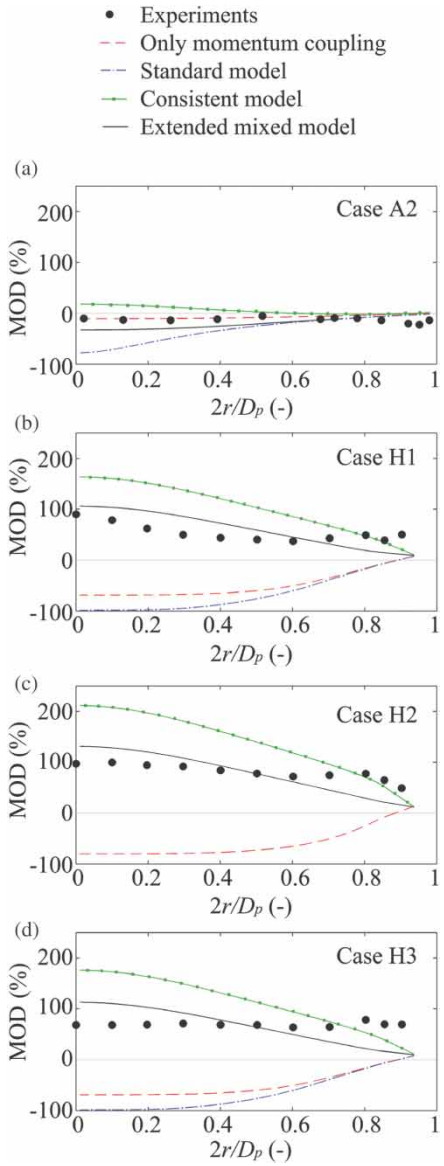

Figure 3 Comparison between numerical predictions and experimental data for the flow conditions A2, H1, H2, H3 in Table 2. The "Experiments" series includes data from Alajbegovic *et al.* (1994) and Hosokawa and Tomiyama (2004)

2010) to consider this parameter as an indicator of turbulence modulation:

$$\mathrm{MOD} = \frac{\phi_f - \phi_{\mathrm{SP}}}{\phi_{\mathrm{SP}}} \tag{19}$$

where ϕ_f is the turbulent intensity of the fluid in the two-phase mixture and ϕ_{SP} is that of an equal flow rate of fluid only. Positive MOD values indicate turbulence enhancements, whereas negative MOD values stand for turbulence attenuations. The turbulent intensity is given as $\phi = u_{\mathrm{RMS}}/U_{\mathrm{ref}}$, where U_{ref} is a reference velocity equal to the superficial velocity of the mixture in order to make MOD dependent upon the turbulent kinetic energy of the fluid (via $u_{\mathrm{RMS}} = \sqrt{2k/3}$) but not upon the local average fluid velocity.

The flow conditions A2, H1, H2, H3 (Table 2), investigated experimentally by Alajbegovic *et al.* (1994) and Hosokawa and Tomiyama (2004), were simulated. The comparison between computations and experiments is reported in Fig. 3 for the four scenarios. The incomplete information about the measured velocity fluctuations forced us to make some simplifying assumptions in the evaluation of $u_{\mathrm{RMS},f}$: as already reported, for the Alajbegovic *et al.* (1994) data, the fluid phase azimuthal and radial velocity fluctuations were supposed to be equal, whilst for the Hosokawa and Tomiyama (2004) ones, $u_{\mathrm{RMS},f}$ was examined in terms of the axial fluctuating velocities. The same assumptions were made by Hadinoto and Chen (2010).

Since one of the peculiar features of our two-fluid model is the evaluation of the source terms in the k and ε equations by means of an extended version of the mixed model of Mandø *et al.*

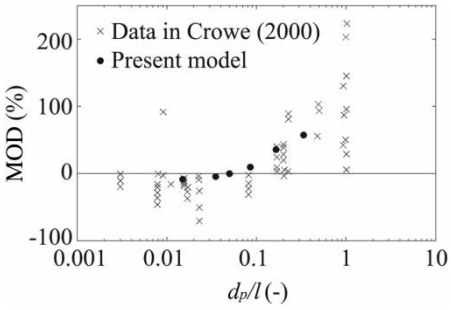

Figure 4 Area-average values of *MOD* versus the ratio of particle size to turbulence scale: predictions of the proposed model and experimental data reported in Crowe (2000)

Table 3 Area-averaged values of *MOD*: comparison between different models for the source terms in the k and ε equations for cases A2, H1, H2, and H3 in Table 2

	Area-averaged MOD (%)				
Case	Experimental	Only momentum coupling	Standard model	Consistent model	Extended mixed model
A2	−12	−6	−19	2	−15
H1	46	−43	−53	85	47
H2	72	−54	–	117	62
H3	69	−49	−53	94	51

(2009) (referred to as "extended mixed model"), the following other alternatives reported in the literature have been explored and the results are shown in Fig. 3: (1) only momentum coupling, i.e. $S_{kp} = S_{\varepsilon p} = 0$; (2) a model based on the standard approach (Eqs. 5 and 6); and (3) a model based on the consistent approach (Eqs. 6 and 7). In all cases, the model of Issa and Oliveira (1997) was employed to evaluate the correlations $\overline{\boldsymbol{u}_f' \boldsymbol{u}_p'}$ and $\overline{\boldsymbol{u}_p' \boldsymbol{u}_p'}$. However, as per the specific indications reported in Mandø *et al.* (2009), the constant $C_{3\varepsilon}$ in Eq. (6) was set to 1.8 in the consistent model and to 1.0 in all other cases.

The results depicted in Fig. 3 highlight that the momentum coupling alone results in a decrease in the fluid RMS velocity, probably as a consequence of the momentum transfer between the phases. Similar results were found also by Mandø *et al.* (2009) for gas–solid flows. The source terms in the k and ε equations produce a variation of the fluid RMS velocity with respect to the "only momentum coupling" case.

The standard model decreases significantly the turbulence intensity of the fluid and predicts turbulent attenuation for cases A2, H1, and H3, contradicting the experimental evidence for the last two cases. For case H2, the standard model produces a complete suppression of turbulence causing the simulation to diverge.

The consistent model determines a significant increase in the fluid RMS velocity with respect to the "only momentum coupling" case. Turbulence enhancements are predicted for all four cases, in disagreement with the experiments for case A2. For the other cases, the predicted MOD values are considerably higher compared with the measured ones.

For all the four flow conditions reported in Fig. 3, the extended mixed model appears capable in correctly predicting whether the RMS velocity of the fluid is attenuated or enhanced by the solid particles. The computed values of MOD are in rather good agreement with the experimental ones from a quantitative point of view especially in the turbulent core region of the pipe, where the proposed model shows the best predictive capacity. All the approaches show relatively a poor performance near the pipe wall, revealing the already observed inadequate modelling of the flow field in the near-wall region. The development of a suitable model for describing the flow of the two phases close to the pipe wall, suitable for embedding in a two-fluid model and possibly accounting for the effect of pipe roughness (which is ignored in this work but whose importance was underlined by Mandø and Jin 2012) may be a challenging goal for future research. In order to allow better comparison, the area-averaged values of MOD obtained by the different models are summarized in Table 3.

The effect of particle size on the turbulence modulation was last investigated by varying the particle size for the flow conditions H2 in Table 2. Figure 4 shows the area-averaged values of MOD as a function of the of particle size to turbulence length scale l. In order to compare our results with the experimental data reported by Crowe (2000), reference is made to his definitions of turbulence intensity ϕ (with U_{ref} equal to the modulus of the average fluid velocity at the pipe centreline) and l equal to 0.10 of the pipe diameter. The results indicate that the model is capable of predicting Crowe's conclusion that "small particles tend to attenuate turbulence, large particles tend to enhance turbulence"; the predictions show the same trends as the data further

confirming the reliability of the proposed model in estimating turbulence modulation.

4 Conclusions

In this work a two-fluid model has been proposed for the simulation of turbulent dispersed liquid–solid flows in vertical pipes. Its focus is the description of the fluid–particle interactions which are extremely significant for these flows. The peculiar features are the modelling of the interfacial momentum transfer terms and of the source terms in the conservations equations for k and ε to account for turbulence modulation. In this regard, a new extended version of the correlations developed by Mandø *et al.* (2009) for gas–solid flows was employed.

By comparison with the experimental data from different authors (Alajbegovic *et al.* 1994, Hosokawa and Tomiyama 2004), the model revealed that it is capable of reproducing the main features of turbulent liquid–solid flows in vertical pipes for different flow conditions without any kind of calibration made on a case-by-case basis. In particular, the extended version of the correlations of Mandø *et al.* (2009) shows promising results for turbulence modulation in liquid–solid flows, procuring a better agreement to the experimental evidence compared with alternative formulations available in the literature. Moreover, it proved capable of reproducing the effect of particle size on turbulence modulation observed in many experiments (Crowe 2000).

Acknowledgement

The authors would like to acknowledge the CINECA and the Regione Lombardia award under the LISA initiative, for the availability of high performance computing resources and support.

Notation

C = area-averaged solid volume fraction (–)
$C_{1\varepsilon}$ = constant in Eq. (15) (–)
$C_{2\varepsilon}$ = constant in Eq. (15) (–)
$C_{3\varepsilon}$ = constant in Eq. (6) (–)
C_d = drag coefficient (–)
C_l = lift coefficient (–)
C_{vm} = virtual mass coefficient (–)
C_μ = constant in Eq. (16) (–)
d_p = particle size (m)
$\mathbf{D}$ = deformation tensor (s^{-1})
D_p = pipe diameter (m)
f = friction factor (–)
$\boldsymbol{g}$ = gravitational acceleration vector (ms^{-2})
J = volumetric flux (ms^{-1})
k = turbulent kinetic energy of the fluid (m^2s^{-2})
l = turbulence length scale (m)
l_m = mixing length (m)
$l_{m,i}$ = mixing length at inlet section (m)
m = parameter in Eq. (17) (–)
m_T = parameter in Eq. (17) (–)
$\boldsymbol{M}$ = interfacial momentum transfer (Nm^{-3})
MOD = turbulence modulation parameter (–)
N = parameter in Table 1 (–)
P = average pressure (Pa)
r = distance from pipe axis (m)
R = Reynolds number based on V and D_p (–)
R_p = particle Reynolds number (–)
R_θ = microscale Reynolds number (–)
S_T = Stokes number based on T (–)
S_θ = particle Stokes number (–)
S_{kp} = source term in k-equation ($Nm^{-2}s^{-1}$)
$S_{\varepsilon p}$ = source term in ε-equation ($Nm^{-2}s^{-2}$)
T = fluid integral time scale seen by a particle in absence of relative velocity (s)
T_e = eddy turnover time (s)
T_E = Eulerian fluid time scale in a frame moving with average fluid velocity (s)
T_L = Lagrangian fluid time scale (s)
u_RMS = RMS velocity (ms^{-1})
$\boldsymbol{u}'$ = fluctuating velocity vector (ms^{-1})
U = average velocity component (ms^{-1})
U_r = modulus of the difference between the average velocities of the phases (ms^{-1})
U_ref = reference velocity (ms^{-1})
$\boldsymbol{U}$ = average velocity vector (ms^{-1})
V = superficial velocity (ms^{-1})
y^+ = dimensionless wall distance of the first grid nodes (–)
z = distance from inlet section (m)
α = average local volume fraction (–)
α' = fluctuating local volume fraction (–)
β = parameter in Eq. (12) (–)
β_T = parameter in Eq. (17) (–)
γ = crossing trajectories parameter (–)
Γ = parameter in Eq. (17) (–)
ε = rate of dissipation of the fluid turbulent kinetic energy (m^2s^{-3})
λ = Kolmogorov length scale (m)
ν = kinematic viscosity coefficient of the fluid (m^2s^{-1})
ν_t = kinematic eddy viscosity (m^2s^{-1})
ρ = density (kgm^{-3})
σ_k = constant in Eq. (14) (–)
σ_α = turbulent Schmidt number for volume fractions (–)
σ_ε = constant in Eq. (15) (–)
τ_p = particle response time (s)
ϕ = turbulence intensity (–)
q = phase indicator (equal to either f or p)
f = of the fluid phase
p = of the particle phase
SP = of the single-phase case
z = along the axial coordinate

References

Alajbegovic, A., Assad, A., Bonetto, F., Lahey, R.T. (1994). Phase distribution and turbulence structure for solid/fluid upflow in a pipe. *Int. J. Multiphase Flow* 20(3), 453–479.

Alajbegovic, A., Drew, D.A., Lahey, R.T. (1999). An analysis of phase distribution and turbulence in dispersed particle/liquid flows. *Chem. Eng. Comm.* 174(1), 85–133.

Assad, A., Bonetto, F., Lahey, R.T. (2000). An experimental study of phase distribution and turbulence structure for solid/liquid flow in a horizontal pipe. *Chem. Eng. Comm.* 179(1), 149–177.

Burns, A.D., Frank, T., Hamill, I., Shi, J.M. (2004). The favre-averaged drag model for turbulent dispersion in eulerian multi-phase flows. Proc. Int. Conf. *Multiphase flow ICMF 2004*, 5, Yokohama, Japan.

Celik, I.B., Ghia, U., Roache, P.J. (2008). Procedure for estimation and reporting of uncertainty due to discretization in CFD applications. *J. Fluids Eng.* 130(7), 078001.

Crowe, C.T. (2000). On models for turbulence modulation in fluid-particle flows. *Int. J. Multiphase Flow* 26(5), 719–727.

Dellavalle, J.M. (1948). *Micrometrics*. Pitman, London.

Di Felice, R. (1994). The voidage function for fluid–particle interaction systems. *Int. J. Multiphase Flow* 20(1), 153–159.

Frawley, P., O'Mahony, A.P., Geron, M. (2010). Comparison of Lagrangian and Eulerian simulations of slurry flows in a sudden expansion. *J. Fluids Eng.* 132, 091301.

Hadinoto, K. (2010). Predicting turbulence modulation at different Reynolds numbers in dilute-phase turbulent liquid-particle flow simulations. *Chem. Eng. Sci.* 65(19), 5297–5308.

Hadinoto, K., Chew, J.W. (2010). Modeling fluid–particle interaction in dilute-phase turbulent liquid-particle flow simulation. *Particuology* 8(2), 150–160.

Hosokawa, S., Tomiyama, A. (2004). Turbulence modification in gas–liquid and solid–liquid dispersed two-phase pipe flows. *Int. J. Heat Fluid Flow.* 25(3), 489–498.

Issa, R.I., Oliveira, P.J. (1997). Assessment of a particle – turbulence interaction model in conjunction with an Eulerian two-phase flow formulation. Proc. Int. Symp. *Turbulence, heat and mass transfer*, 2, Delft, K. Hanjalic, T.J. Peeters, eds. Delft. Univ. Press. Dup. Sci., Delft NL, 759–770.

Lain, S., Sommerfeld, M. (2003). Turbulence modulation in dispersed two-phase flow laden with solids from a Lagrangian perspective. *Int. J. Heat Fluid Flow* 24(4), 616–625.

Launder, B.E., Spalding, D.B. (1972). *Mathematical models of turbulence*. Academic Press, London.

Lightstone, M.F., Hodgson, S.M. (2004). Turbulence modulation in gas-particle flows: A comparison of selected models. *Can. J. Chem. Eng.* 82(2), 209–219.

Loth, E. (2011). *Particles, drops and bubbles: Fluid dynamics and numerical methods.* Draft for Cambridge University Press. To be published.

Mandø, M., Yin, C. (2012). Euler–Lagrange simulation of gas–solid pipe flow with smooth and rough wall boundary conditions. *Powder Technol.* 225, 32–42.

Mandø, M., Lightstone, M.F., Rosendahl, L., Yin, C., Søresen, H. (2009). Turbulence modulation in dilute particle-laden flow. *Int. J. Heat Fluid Flow* 30(2), 331–338.

Nouri, J.M., Whitelaw, J.H., Yianneskis, M. (1987). Particle motion and turbulence in dense two-phase flows. *Int. J. Multiphase Flow* 13(6), 729–739.

Pepple, M. (2010). Benchmark data and analysis of dilute turbulent fluid-particle flow in viscous and transitional regime. *PhD Thesis*. Department of Chemical Engineering, University of Florida, FL.

Pinelli, D., Montante, G., Magelli, F. (2004). Dispersion coefficients and settling velocities of solids in slurry vessels stirred with different types of multiple impellers. *Chem. Eng. Sci.* 59(15), 3081–3089.

Sad Chemloul, N., Benrabah, O. (2008). Measurement of velocities in two-phase flow by laser velocimetry: Interaction between solid particles' motion and turbulence. *J. Fluids Eng.* 130(7), 071301.

Schlichting, H. (1960). *Boundary layer theory*. McGraw-Hill, New York.

Spalding, D.B. (1972). A novel finite-difference formulation for differential expressions involving both first and second derivatives. *Int. J. Num. Meth. Eng.* 4(4), 551–559.

Spalding, D.B. (1980). Numerical computation of multi-phase fluid flow and heat transfer. In *Recent advances in numerical methods in fluids*. C. Taylor, K. Morgan, eds. Pineridge Press Limited, Swansea, 139–168.

Zisselmar, R., Molerus, O. (1979). Investigation of solid–liquid pipe flow with regard to turbulence modification. *Chem. Eng. J.* 18(3), 233–239.